



FLOW VISUALIZATION OF ROTOR WAKES
USING SHADOWGRAPH AND SCHLIEREN TECHNIQUES

BY

ERWIN MOEDERSHEIM, MARK DAGHIR AND J. GORDON LEISHMAN

CENTER FOR ROTORCRAFT EDUCATION AND RESEARCH
DEPARTMENT OF AEROSPACE ENGINEERING
UNIVERSITY OF MARYLAND AT COLLEGE PARK
MARYLAND 20742, USA

TWENTIETH EUROPEAN ROTORCRAFT FORUM
OCTOBER 4 - 7, 1994 AMSTERDAM

FLOW VISUALIZATION OF ROTOR WAKES USING SHADOWGRAPH AND SCHLIEREN TECHNIQUES

Erwin Moedersheim* Mark Daghir† J. Gordon Leishman‡

Center for Rotorcraft Education and Research,
Department of Aerospace Engineering,
University of Maryland at College Park, Maryland 20742, USA.

ABSTRACT - A series of shadowgraph and schlieren studies were performed to visualize the wakes of small scale rotors operated at tip Mach numbers between 0.5 and 0.9. The objectives were to examine the relative merits of both techniques in an attempt to gain a better appreciation of the various flow problems that could be studied on rotors, possibly on a larger scale. Various optical and photographic techniques were also explored, with a view to optimizing the techniques for rotor applications. Studies were conducted in hover and descent with various propellers and rotors. Rotor wake/body interactions were also examined using cylindrical body shapes.

NOMENCLATURE

a	Unobstructed height of schlieren light source in cutoff plane, m	c	Blade chord, m
f	Focal length of schlieren focusing mirror, m	C_T	Rotor thrust coefficient, $T/(\rho\pi\Omega^2 R^4)$
I	Image screen illumination, cd	l	Distance from vortex to shadowgraph screen, m
n_b	Number of blades	R	Rotor radius, m
T	Rotor thrust, N	v_c	Climb velocity, m/s
v_h	Averaged hover induced velocity, m/s	Γ_∞	Circulation (strength of vortex), m^2/s
η	Refractive index of fluid medium	η_0	Refractive index of fluid medium at reference conditions
κ	Gladstone-Dale constant, m^3/kg	ρ	Density, kg/m^3
ρ_∞	Density at ambient conditions, kg/m^3	σ	Rotor solidity, $(n_b c/\pi R)$
Ω	Rotor rotational frequency, rad/s		

1. INTRODUCTION

The flow fields of propellers and helicopter rotors are laden with several significant phenomena that have important effects on performance, loads, and noise. While the most dominant flow features are the vortices generated near the tips of each blade, other significant flow structures include the formation of shock waves at the blade tips, and large amounts of turbulence behind each blade. On rotors, the tip vortices are convected through the flow with complex interlocking trajectories. These tip vortices produce relatively high peak peripheral velocities (approximately one-half the rotor tip speed), and this induced velocity field directly affects rotor performance, blade loads and acoustics. An understanding of the location, strengths and structure of the tip vortices is especially important for situations such as blade/vortex interaction (BVI), which are known to produce locally high blade loads and impulsive noise.

There have been several experiments conducted to document the wake geometry and induced velocity field for rotors. Various experimental methods have been used including probes, hot-wires and laser Doppler velocimetry (LDV), see for example Boatwright,¹ Caradonna and Tung,² and Biggers.³ The first comprehensive wake surveys below a rotor in forward flight were performed by

*Graduate Research Assistant.

†Graduate Research Assistant.

‡Associate Professor.

Presented as paper No. 31, 20th European Rotorcraft Forum, Amsterdam, The Netherlands, 4-7 October 1994.

Heyson and Katzoff using five-hole probes.⁴ Other measurements of rotor induced velocities have also been obtained by Cheeseman and Haddow,⁵ and Leishman and Bi.⁶ Increasing amounts of data documenting the unsteady nature of the flow have become available through the use of hot-wire anemometry, e.g. Ref. 7 and LDV techniques, e.g. Refs. 3 and 8. Particular attention has been placed on measuring the detailed structure the tip vortices. Cook,⁹ Tung *et al.*¹⁰ and others, have used hot wire anemometry for this purpose.

Flow visualization methods also allow considerable information to be derived about the structure of rotor wakes. Light sheet techniques have been used for many years to visualize the locations of vortical structures in wing, rotor and propeller wakes, e.g., see Piziali and Trenka,¹¹ Spencer,¹² Leighty *et al.*,¹³ Ghee and Elliott.¹⁴ A dense white smoke efficiently reflects the light allowing a photographic exposure of the flow structure to be recorded. Natural condensation of water vapor in the tip vortices produces clear evidence of the location of tip vortices – see Ref. 15. Optical density gradient methods of flow visualization such as shadowgraphy and schlieren can also be used to examine rotor wakes. Density gradient flow methods have certain advantages since they are completely non-intrusive and seed particles are not required to reflect light and create the photographic image. However, a fundamental requirement is that the flow field contain elements with a density inhomogeneity. While the density gradients associated with shock waves are significant, this is not always the case with vortical fields. Yet, propellers and rotors operating at sufficiently high tip speeds and thrusts are known to produce compressible vortices of sufficient strength to cause density variations making density gradient flow visualization techniques such as shadowgraphy and schlieren feasible – see Hilton,¹⁶ Tangler,¹⁷ Norman and Light¹⁸ and more recently Bagai and Leishman.¹⁹ However, for various reasons these techniques have not yet found widespread use for rotor wake visualization.

The simplest density gradient method of flow visualization is direct shadowgraphy. Here, refraction effects in regions of density inhomogeneity cause shadows of the flow field to be cast directly onto a recording screen. Typically, a shadowgraph of a rotor wake consists of thin dark strands, generally surrounded by bright bands, which identify the presence of the tip vortices. Other structures such as turbulence and shock waves have also been observed in shadowgraph experiments on propellers and rotors, e.g., Hilton,¹⁶ Bagai and Leishman.¹⁹ While no quantitative measurements of the flow field properties are possible, shadowgraphy allows the location of the density variation to be located in space. In fact, fairly extensive measurements of the tip vortex trajectories relative to the rotor plane have been made using these methods, e.g., see Parthasarathy *et al.*,²⁰ Norman and Light,¹⁸ Light.²¹ The technique has also been used by Leishman and Bagai²² to measure the geometry of rotor wakes in forward flight.

The schlieren technique is somewhat more complicated in practical application since it requires the use of focusing mirrors and/or lenses. The expense involved in using high quality components free of optical defects usually limits the diameter of the field of view to less than 0.5 meters. Nevertheless, for some applications schlieren is considered more useful since it is sensitive to the first spatial derivative of the density field compared to the shadowgraph which is sensitive to the second. Tangler¹⁷ has used the schlieren method to examine the development of three-dimensional shock waves on small-scale rotors, with quite dramatic results. However, the technique has not found widespread use for rotor studies because of the difficulty of positioning optical elements in wind tunnels and the narrow field of view. Nevertheless, with the increasing emphasis on understanding of tip vortices, shock waves, and acoustic radiation from rotors, it was felt necessary to reexamine this technique for rotor applications.

To this end, this paper presents some results in which shadowgraph and schlieren methods were employed to investigate the flow field from rotors and propellers. To conduct these experiments, a portable small-scale high speed rotor rig was designed and built. Although of a small-scale, this rotor permitted realistic tip Mach numbers of 0.5 to 0.9 to be attained. One goal was to use the results from these tests as a guide to explore the feasibility of more effectively using these techniques for rotor flow field studies on a larger scale.

2. SHADOWGRAPH AND SCHLIEREN METHOD

Both the shadowgraph and schlieren methods are concerned with the refraction of light produced by local density variations in the flow field. The refractive index, η , of the flow is related to the fluid density, ρ , of a homogeneous transparent medium by

$$\left(\frac{1}{\rho}\right) \frac{\eta^2 - 1}{\eta^2 + 2} = \text{constant} \quad (1)$$

Since for most gases (including air) $\eta \approx 1$, Eq. 1 can be reduced to

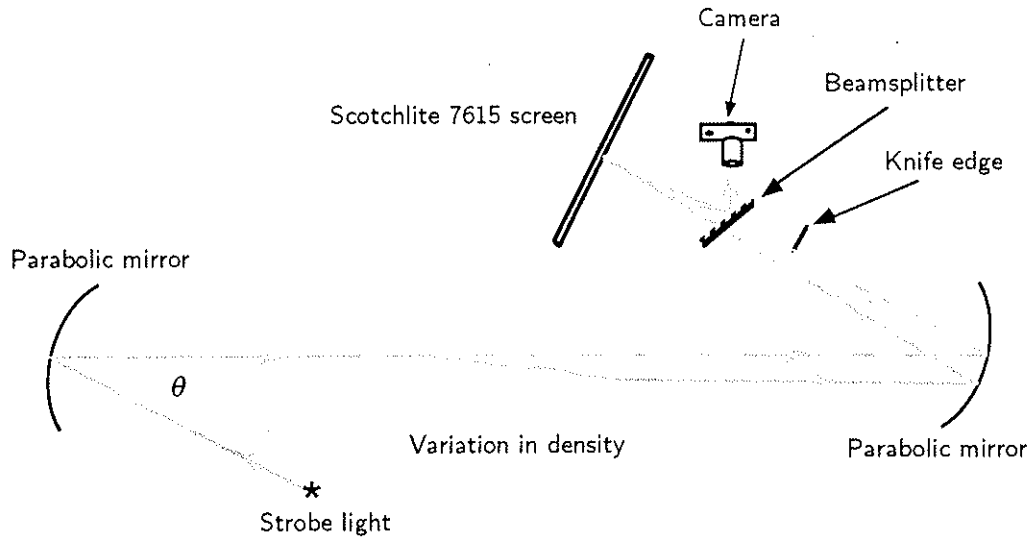


Figure 1: Schlieren set-up

$$\eta = \kappa\rho + 1 \quad (2)$$

with sufficient accuracy. The Gladstone-Dale constant, κ , varies with both the fluid medium and the wavelength of the incident light. For air at standard pressure and density, the refractive index can be assumed to depend only on the wavelength of the incident light.

Schlieren Set-up

It will be seen from Eq. 2 that the refractive index of the fluid is directly proportional to its density. Therefore, if there are planes of density variation in the flow field, incident light rays normal to the plane will be refracted. The contrast or distribution of light intensity due to density variations that would be obtained in the Toepler schlieren method can be written as

$$\frac{\Delta I}{I} = \frac{f}{a} \int_{l_1}^{l_2} \left(\frac{\partial \eta}{\partial y} \right) dz = \frac{f\kappa}{a} \int_{l_1}^{l_2} \left(\frac{\partial \rho}{\partial y} \right) dz \quad (3)$$

where l_1 to l_2 is the light path length through the density variation. Therefore, the angular deflection of these light rays is a measure of the first derivative of density with respect to distance, and can be observed by several well-known schlieren techniques that employ focusing lenses or mirrors.

A typical schlieren set-up used for the present experiments is shown in Fig. 1. Here, light is emitted from a source placed at the focal point of a parabolic mirror. The first mirror reflects the light as a collimated beam into the flow field where some of the light rays are refracted in regions of density inhomogeneity. For rotor experiments, the strobe must be synchronized to the rotor frequency to produce a single illumination of the flow field for each rotor revolution. The light is then gathered by a second parabolic mirror, and converges at the focal point of this mirror. A knife edge at this focal point is adjusted so that the light refracted in one direction is cut off. As a result, only light with a refraction component perpendicular to the knife edge in one direction passes through undisturbed. Light refracted parallel to the knife edge is cut-off equally regardless of the amount of refraction, thereby negating the effect of the knife edge. Consequently, the knife edge must be positioned perpendicular to the direction in which the density gradients are to be observed. After the knife edge, the light passes through a beam-splitter, and is projected on the ScotchliteTM 7615 screen. This image is reflected by the beam splitter to the camera. Further details of various schlieren set-ups can be found in Ref. 23.

Shadowgraph Set-Up

If the refractive index also varies in the plane, the deflections of adjacent light rays will vary. This will produce diverging or converging light rays, and if cast onto a projection screen, will result in relative displacements of the light rays, by that producing regions of decreased or increased illumination. This is the basis of the Dvorak's direct shadowgraph method.

The contrast on a shadowgraph screen due to the refraction of light rays can be written as

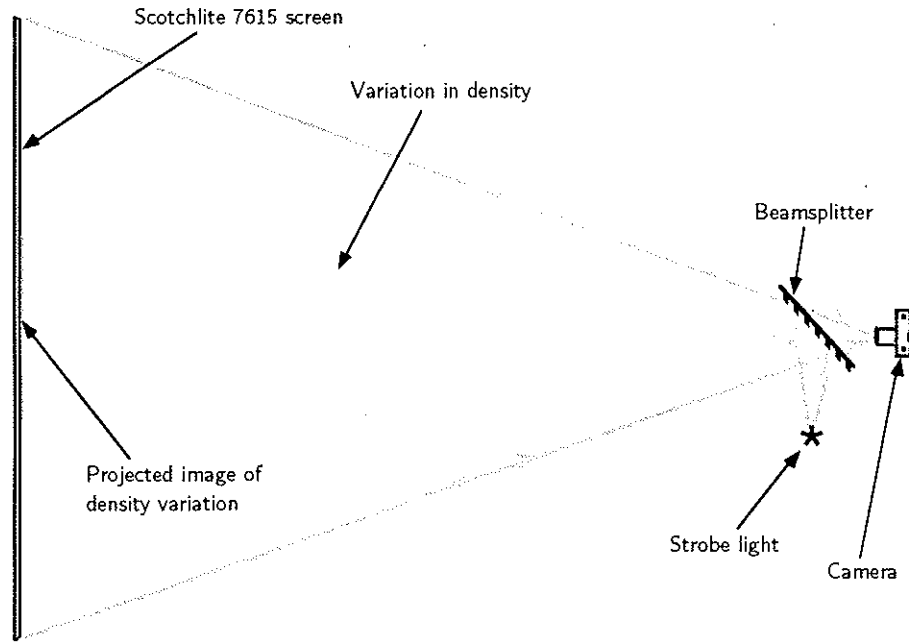


Figure 2: Shadowgraph set-up

$$\frac{\Delta I}{I} = -\frac{l}{\eta_0} \int_{l_1}^{l_2} \left(\frac{\partial^2 \eta}{\partial x^2} + \frac{\partial^2 \eta}{\partial y^2} \right) dz = -\frac{l\kappa}{\eta_0} \int_{l_1}^{l_2} \left(\frac{\partial^2 \rho}{\partial x^2} + \frac{\partial^2 \rho}{\partial y^2} \right) dz \quad (4)$$

where we see that now the effects observed vary with the second derivative of the density field. Note also that the shadowgraph contrast depends on the distance from the light source to the screen, l , while the schlieren contrast does not.

The shadowgraph set-up used here was optimized for large angles of view, similar to the set-up used previously by Bagai and Leishman,¹⁹ see Fig. 2. The light from the strobe is first transmitted through a beam-splitter* and into the flow field. As the light rays encounter the nonuniform density in the flow field they are deflected from their original paths, and produce a non-uniform illumination on the projection screen, which is the shadowgraph image. These light rays are reflected back through the flow field and beam-splitter, and the image is recorded by the camera.

It will be clear that a major advantage of the shadowgraph method is that the investigator is not as limited in angle or field of view compared to the schlieren method. The extent of the flow field to be visualized is determined by the angle of view (distance from light source to screen) and the actual size of the screen. However, for large angles of view the shadowgraphic image on the screen can be magnified several times (depending on the source/screen distance) and this can limit the field of view.

3. DESCRIPTION OF THE EXPERIMENT

Rotor Rig

The extent of the experiments planned required high versatility from the rotor rig. Among the characteristics required were mobility, simplicity of use, adaptability, low operating cost, and a large tip speed range. The rotor rig was built around a Task Corporation water cooled three-phase motor (model 2751-2). This motor was only 152 mm in length and 55 mm in diameter, but was capable of delivering 4.5 kW at rotational speeds up to 400 Hz (24,000 RPM). A variable frequency controller (Polyspede model VXT-75FG inverter) was used to power the motor.

The rotor shaft was connected to the motor by a Lovejoy U-37 universal coupling. The shaft was supported at two points by Barden 103SST-G6 high speed bearings, with a pair located at one point and a single bearing at the second. The rotor or propeller was mounted directly onto the end of the shaft. The complete assembly of motor, coupling, and bearings was mounted inside a purpose built aluminum housing, with appropriate mounting attachments.

*For best results, the beam-splitter should have an anti-reflective coating.

An infrared sensor was located inside the motor housing to serve as a 1/rev signal. This signal was used to measure the rotor speed and calculate the tip Mach number. It was also used to trigger the strobe lamp. The strobe frequency was reduced electronically to 1/2 rev, 1/4 rev or 1/8 rev, which was necessary to obtain a frequency within the range of acceptable camera shutter speeds.

All systems were interfaced to a Macintosh Quadra 950 computer. A LabVIEWTM program was written to start and stop the motor, control rotor speed and monitor tip Mach number, and check motor performance. This allowed the investigator to obtain a continuous record of the test, with data being taken about every two seconds. An optional strain gage attachment containing two full Wheatstone bridges allowed measurement of the rotor thrust.

Optical System

The light source used for both the shadowgraph and schlieren studies was a Chadwick-Helmuth Slip-Sync Strobex system with a strobe employing an Advanced Radiation Corporation model 35S flashtube. The lens and reflector were removed from the lamp housing to provide a point light source. For the schlieren experiments, a set of parabolic mirrors 0.25 m in diameter were used. The mirrors had focal lengths of 2050 mm and 1520 mm respectively, but this difference in focal length is not critical to the experiment if the strobe and knife edge are placed as close as possible to the focal points of each mirror. It is crucial to keep the angle between the center of the collimated light beam and the strobe light to a minimum. If this angle is not kept small, an aberration termed astigmatism can occur, and it will become impossible to focus the light beam at the knife edge. Another effect called coma can result in a contrast gradient across the schlieren image. This is again the result of placing the elements off the optical axis of the system. Here, the light rays reflected from the top of the first mirror are reflected at a slightly different angle than the beams from the bottom of the mirror, resulting in a contrast gradient. Coma can be reduced by similarly aligning the mirrors in a Z-configuration so that the coma effects of each mirror cancel.

For the shadowgraph tests, the screen material is critical. The screen used here was made of 3M ScotchliteTM 7615, which is a high contrast retroreflective film. This screen reflects incident light directly back to its source for light rays within a certain angularity, and has a reflectivity of about one-thousand times higher than a white background. Note that the use of a beam splitter allows the light source and camera to be effectively collocated on the optical axis of the system, and maximizes the retroreflective properties of the screen. The beam-splitter also alleviates several other optical problems associated with large angles of view.¹⁹ However, it is still not recommended to view the shadowgraph screen at very large incident angles (greater than 30 degrees). Despite the excellent retroreflective characteristics of the ScotchliteTM film, a drop in intensity is observed for large incident angles, which like coma, appears as a contrast gradient.

Experimental Approach

The configurations utilized in the experiments ranged from a one-bladed rotor to a series of propellers. Experiments with the one-bladed rotor documented the effects of different rotor radii up to 0.46 meters and with different twist distributions. The tip Mach numbers during the experiments varied from 0.5 to 0.9, depending on the rotor configuration. The rotors were tested in both hover and axial descent conditions. Tests were also conducted with a cylindrical body in the flow to simulate the interaction of the rotor wake with an airframe.

In hover state, the rotor was mounted on a tower with the rotor thrusting down. Therefore, the wake was allowed to develop completely unimpeded by wall constraints. The strobe light was synchronized to a sub-multiple of the 1/rev from the rotor shaft encoder. Adjusting the phase angle of the strobe relative to the rotor position provided flow field images at various rotor azimuth angles. Since the flow in hover is essentially axisymmetric, the entire three-dimensional structure of the wake could be examined from a single viewing angle parallel to the rotor plane. However, a limited number of flow field images were obtained from the top perspective (viewing perpendicular to rotor plane) to check for the presence of acoustic disturbances.

An interesting perspective on the dynamics of the wake can be obtained by continuously slipping the phase of the strobe relative to the rotor. This created, in effect, a slow-motion animation of the wake development. A high-resolution B&W video camera was used to record this image. Several hours of video were recorded during the experiments.[†]

To study the rotor wake structure in the descent condition, the rotor was mounted on a horizontal fixture in front of a free-jet wind tunnel. The tunnel was set to various velocities to simulate an

[†]Extracts from this video are available from the authors upon special request.

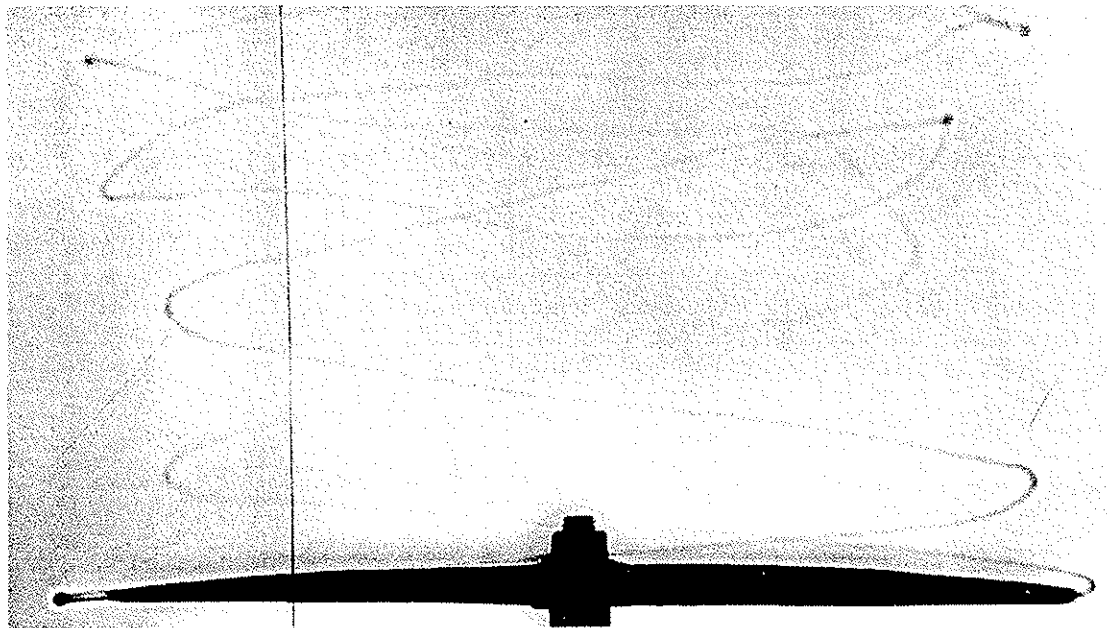


Figure 3: Sample shadowgraph (propeller in hover), $M_{tip} = 0.68$

axial descent while the rotor tip speed was fixed at a constant Mach number. Particular attention was paid to simulating the so-called vortex-ring state, since very little detailed flow visualization has previously been done on this problem.

4. RESULTS AND DISCUSSION

Hover

The first series of tests involved the use of various fixed-pitch propellers operating in hover. Several types were used, such as two-bladed propellers varying from 25-15 cm (25 cm radius with 15 cm pitch per revolution) to 40-20 cm, and a three-bladed 30-20 cm propeller. The propellers were manufactured out of fiberglass-reinforced nylon, and were carefully tracked and balanced prior to the tests.

A sample shadowgraph of a propeller wake in hover is shown in Fig. 3. A schlieren image of a one-bladed rotor wake is shown in Fig. 4. In both cases, the tip vortices appear as thin dark spirals that trail from the blade tips. For the hovering case, the vortices initially follow almost helical trajectories, but ultimately instabilities begin to form. This could be seen as small regular waves on the vortex filaments. For older vortices (more than 3-4 rotor turns), the onset of viscous diffusion reduces the density gradients, and the image was found to become much less visible.

Note that the detailed contrast variations of the tip vortices between the shadowgraphs and schlieren are different; in the latter an asymmetric contrast is produced when viewing a tip vortex, whereas in the shadowgraph case an axisymmetric contrast is produced. For most tests, it was possible to track the tip vortices below the rotor for at least 4 rotor revolutions. In some cases, as many as 8 complete rotor revolutions of wake could be observed. A three-bladed propeller was used for some tests. This yielded similar results to the two-bladed propeller, but the helical pitch of the tip vortices was much less. This also resulted in a somewhat larger amount of distortion to the wake trajectories compared to the two-bladed propeller.

When viewing the flow structure parallel to the disk, what appears to be a vortex sheet in the form of a turbulent wake could be observed behind each blade. An example of this is shown in Fig. 5. In this shadowgraph, the view is almost along the axis of the rotor blade, so the integrated refraction effects through the vortex sheet are quite noticeable.

One of the most obvious observations from these experiments was that the contrast of the shadowgraph/schlieren image (i.e., the strength of the vortices) depended on the rotor thrust. At tip Mach numbers below $M = 0.3$, when little thrust is being generated, no vortices were observed. Weak vortices appeared as the tip speed was increased to above $M = 0.3$, and the strength of the vortices continued to increase with increasing tip Mach number. Note that the approximate strengths of the tip vortices generated in the axial flight condition can be obtained using $\Gamma_{tip} = kc\Omega R(C_T/\sigma)$ where C_T/σ is the blade loading and, theoretically, $k = 2$ for a hovering rotor. In most cases, the tip vortex strengths were between 1.0 and 2.0 m^2/s . It was also observed that propellers with a lower

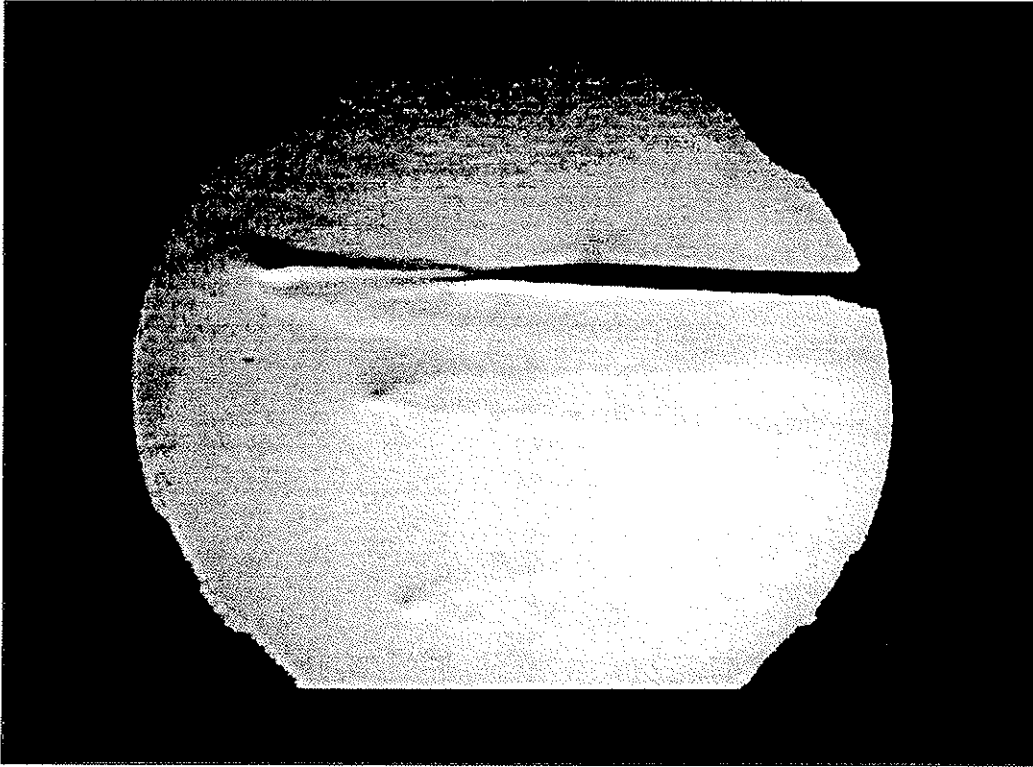


Figure 4: Sample schlieren image (one-bladed rotor) showing tip vortex formation and compressibility zone near leading-edge of blade tip, $M_{tip} \approx 0.7$.

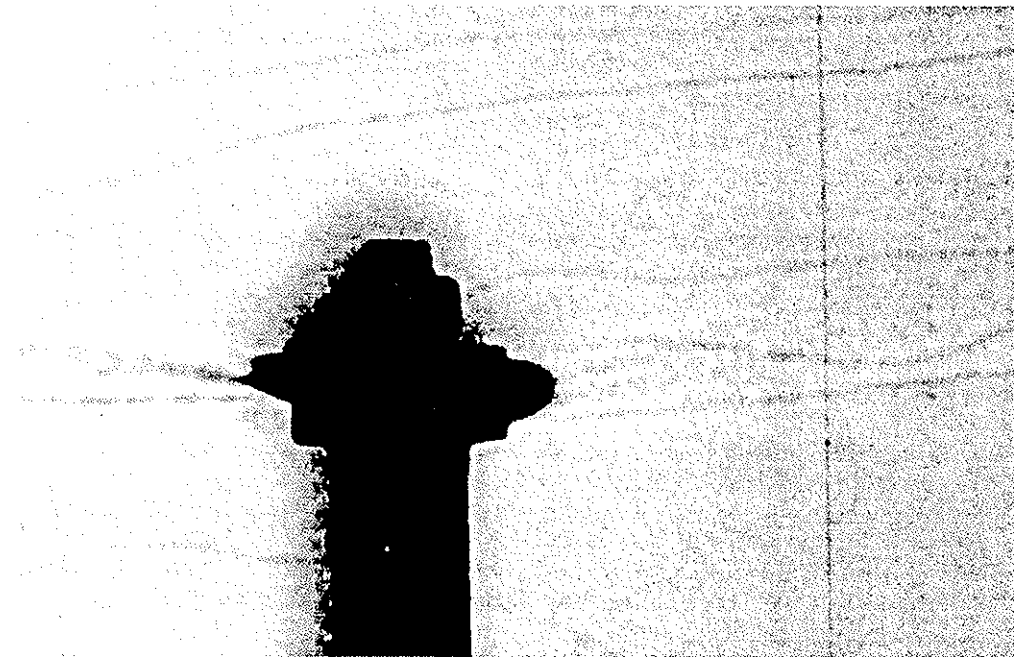


Figure 5: Shadowgraph of vortex sheet from rotor blade, $M_{tip} = 0.63$

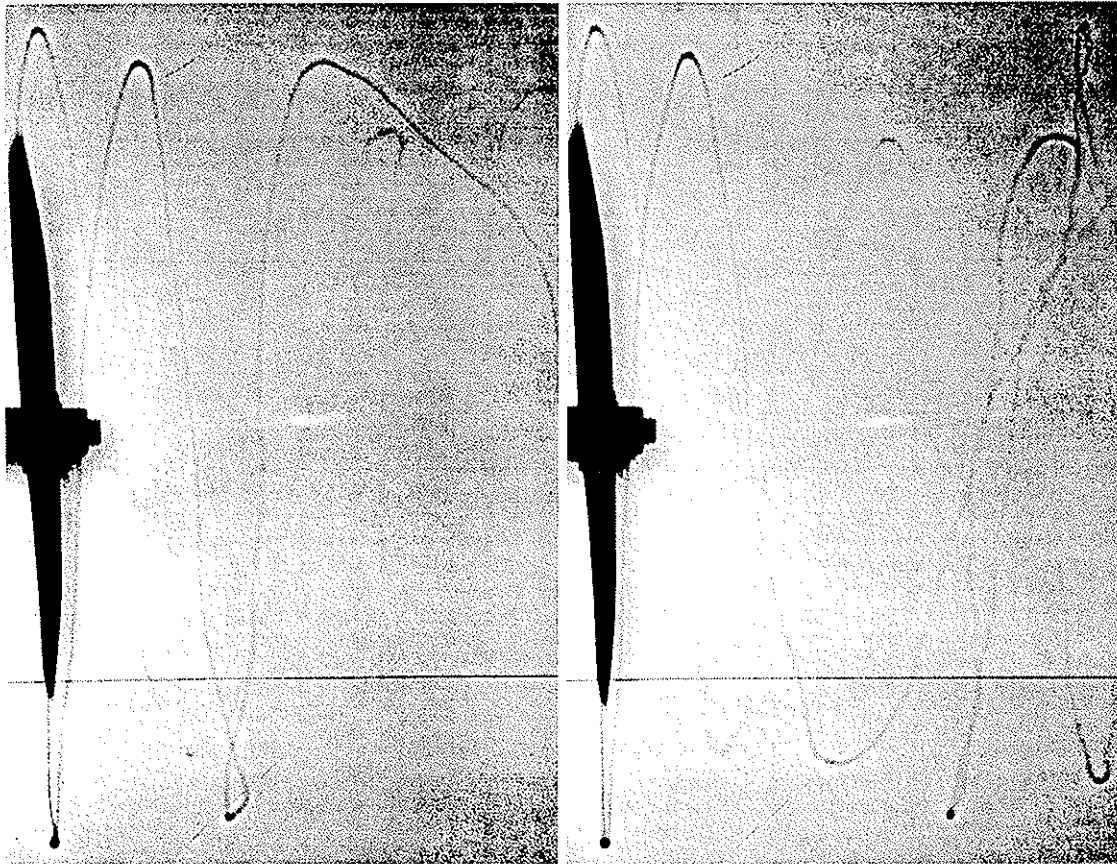


Figure 6: Shadowgraph of bi-stable flow state of hovering rotor, $M_{tip} = 0.70$

pitch created weaker vortices than the medium pitch, since the thrust was lower for a given rpm. However, highly pitched propellers such as 28 cm did not result in observable vortices since the local blade incidences were high enough to produce stall before reaching a sufficiently high thrust.

An interesting phenomenon occurred when the 30-15 propeller was used. Here, the wake appeared to toggle between two stable flow states, with a regular period of about 2 seconds (400-500 rotor revolutions). In one state, the wake took on a regular helical trajectory. In the other state, there was considerably more distortion to the wake trajectories. This bi-stable flow state was particularly evident when the visualized wake was recorded on video. Shadowgraphs of both states of the wake for a given tip Mach number are shown in Fig. 6. Note that test conditions were identical to those used for other propellers, so the phenomenon was clearly propeller specific. It was suggested that a possible cause may be the asymmetry of the propeller blades, yet one would expect this modification to result in a modified stable wake, not a bi-stable wake. While various other theories have been suggested, the reasons for this unique periodic bi-stable behavior of the wake remain to be properly understood.

Photographic Techniques

One purpose of the present experiments was to examine various photographic techniques that could be used to improve the quality of the shadowgraph and schlieren images. First of all, note that by using a beam-splitter, the camera and light source can be collocated on the optical axis of the system. Despite the loss of light intensity produced by each passage through the beam-splitter, on-axis viewing maximizes the retroreflective characteristics of the ScotchliteTM film allowing several times the light intensity obtained at the camera compared to off-axis shadowgraph systems used by others.^{18, 21} This permits the use of 200 ASA to 400 ASA films, which have reasonably fine grain and give excellent contrast. This approach also gives some aperture latitude when high quality lenses are used, such as the Nikon 80-200 mm $f/2.8$ and 35-70 mm $f/2.8$, which were used in the current experiments.

In recording shadowgraphic or schlieren images using a strobe light source, the exposure time is determined by the duration of the strobe flash, rather than the camera shutter itself. Typically

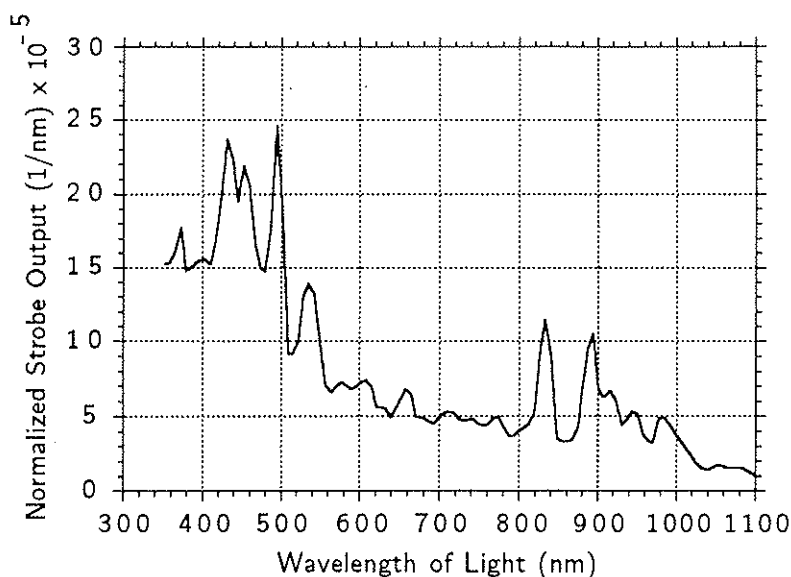


Figure 7: Spectrum of strobe light

this is of the order of 8-15 μ s, depending on the flash frequency. In most experiments, the rotor was operated at speeds near 240 Hz (14,400 rpm), and the strobe was flashed at 0.25/rev (i.e., once every four revolutions). This ensured maximum light energy out of the Slip-Sync unit and strobe lamp, which had an energy output per flash of 1.25 J for frequencies below 62 Hz, but only 0.25 J above 131 Hz. Consequently, the shutter speed could be selected so that only one strobe flash was recorded in each exposure, e.g. 1/60 s. If the background light level is sufficiently low, the resulting exposure time is equal to the flash duration.

Xenon flashtubes such as the model 35S used in the current experiments are commonly used for photography, and their spectral output closely matches the daylight spectrum. This can be demonstrated if Kodak Kodacolor 400 (GC-135) color print film is used to make schlierens or shadowgraphs. The resulting images are neutral gray, rather than a specific color. Exposing the same film under incandescent light would result in a red/brown haze, while neon light would result in a green haze. Since the resulting shadowgraph/schlieren images are essentially gray, it is best to use 400 ASA black-and-white films. It has also been found useful to shoot a roll of Polaroid Polagraph (HC-135) instant slide film before a test on a new configuration, since this will give almost an immediate indication of the correct exposure.

To obtain the best quality recorded images it can be useful to match the sensitivity spectrum of the photographic film used to the light source. This way full advantage can be taken of all light energy arriving at the camera. The spectral output for a typical xenon short arc flashtube is plotted in Fig. 7. While the spectral output of the flashtube varies with current density and frequency,²⁴ this plot is considered representative of the model 35S. The spectral sensitivity of several common black and white films is plotted in Fig. 8 (taken from Refs. 25 through 29). Note that sensitivity is defined as $D = \log_{10}(T_0/T)$ where T_0 is the intensity of the light incident on the negative and T is the intensity of the light transmitted through the negative. The density for this plot is $D = 0.30$ for Kodak films, but is unknown for the Ilford films. The plot shows that most 400 ASA black and white films have roughly the same spectral sensitivity. The spectral sensitivity curves for other films, like Fuji Neopan 400, look similar. Only Ilford XP2 has a sensitivity peak in the same range as the largest peak in the strobe spectral output. This film also has exceptionally fine grain, and is well suited for recording shadowgraphs and schlierens. However, it requires a more complicated C-41 developing process used for most color films.

It is interesting that the strobe output spectrum in Fig. 7 also reveals a peak in the infrared range. This warranted examination of the benefits of using infrared sensitive film. Since shadowgraphy and schlieren usually requires a high speed film, Kodak High Speed Infrared film (HIE-135) was tried. This film does not have the large drop in sensitivity exhibited by normal black and white films, as illustrated in Fig. 9 (taken from Refs. 27 and 29). The film should, therefore, be able to capture some additional information. However, the use of infrared film produces some problems. The primary problem is focus. Because infra-red light has a longer wavelength, it is focused farther away from the lens than visible light rays. In practice, it is hard to obtain a perfectly focused image with infra-red film, and most of the visible light must be filtered out using a red filter to avoid blurring of the infrared image. This results in a slight exposure loss. The film is also considerably coarser

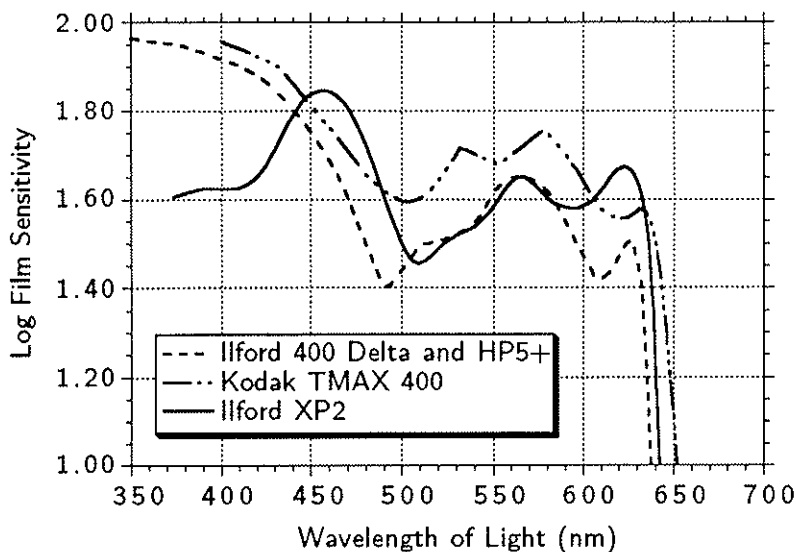


Figure 8: Sensitivity of various B & W daylight films

grain than regular black-and-white films. In addition, infrared film is rated at about 200 ASA for shadowgraph/schlieren purposes, leaving the investigator with little latitude for exposure. In the present tests, it was necessary to push the film a stop to compensate for the use of a filter, which destroyed the contrast of the film and increased its grain. The film was also tested without filter and with a yellow filter. The results without filter yielded slightly better contrast than conventional black and white film, but were not sharp enough to justify routine use of the HIE-135 film.

Rotor-Body Interactions

An investigation was conducted to study the interactions between the rotor wake and a series of cylindrical bodies. The problem of rotor/airframe interference has received considerable attention in recent years,^{30, 31} but there is still a relatively poor understanding of the mechanisms involved. In particular, the impingement of discrete tip vortices on the airframe surface is known to produce large unsteady pressure loads, with the possibilities of corresponding adverse pressure gradients producing flow separation. The detailed fluid mechanics of the vortex filaments during this process are relatively unknown, however, previous work³¹ has shown that there is considerable distortion and straining of the filament as it approaches the surface of the airframe. It has also been suggested by some workers that the tip vortex filaments are "cut" by the airframe, and the ends ultimately undergo some form of reconnection below the airframe.

To study this problem, a fixture was designed to support a cylindrical body in the wake of the rotor. The ratio of the rotor diameter to the body diameter was selected to be typical of a helicopter rotor and airframe. The body supports were located far enough away from the rotor so that only the body itself would aerodynamically interfere with the rotor wake. Two bodies were used: one with a 2.54 cm diameter and a second with a 1.91 cm diameter. Both bodies were painted matte-black to avoid reflections of the strobe light in the shadowgraph image. The bodies were suspended horizontally above the propeller, such that they were inserted half-way into the rotor wake. The resulting interactions were observed from both longitudinal and lateral views. A 30-12 cm propeller was used for all experiments, with the tip Mach number set to 0.70, and with C_T/σ approximately 0.12.

Figs. 10 and 11 show shadowgraphs that document a typical interaction between the tip vortices and the body. In this shadowgraphs, the rotor is thrusting down, such that the wake is moving upward. Note that the vortex is formed at the tip of the rotor blade and is convected upward toward the body. As the vortex approaches the top of the body surface, its vertical convection velocity is retarded and a local deformation is introduced into the filament. A series of images viewed along the longitudinal axis of the body (Fig. 12) clearly showed that the vortex filament stretched around the circular contour of the body, but stood off the surface about 10 to 15% of body radius. Simultaneously, the filament was convected in a direction parallel to the longitudinal axis of the body, so the net effect was the development of a loop or "hairpin" type of filament.

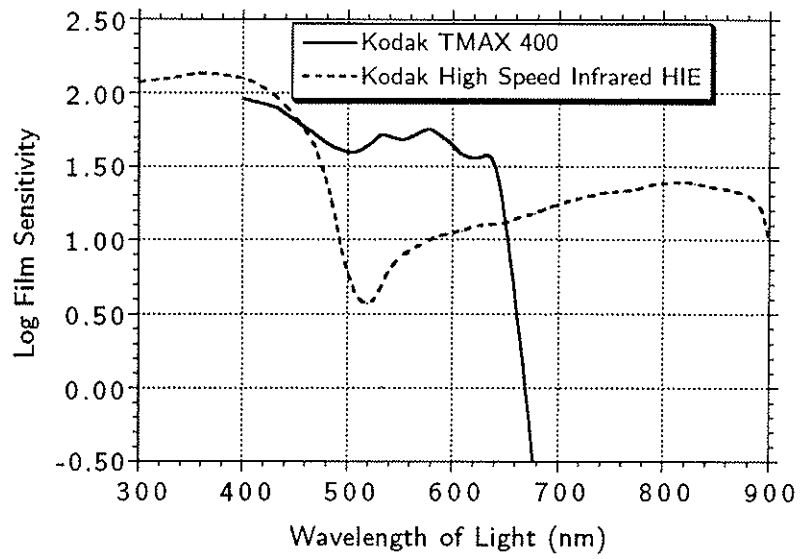


Figure 9: Sensitivity of B & W daylight and infrared films

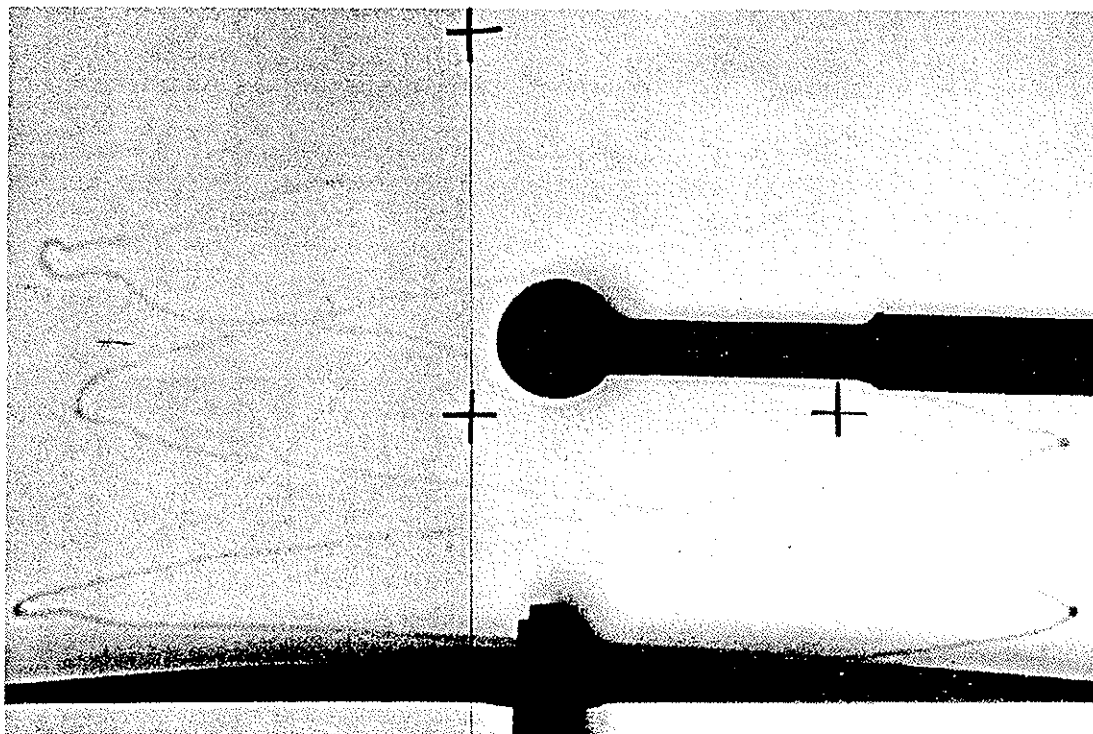


Figure 10: Shadowgraph of rotor tip vortex/body interaction (view along longitudinal axis of body). Early time: Note vortex stretching.

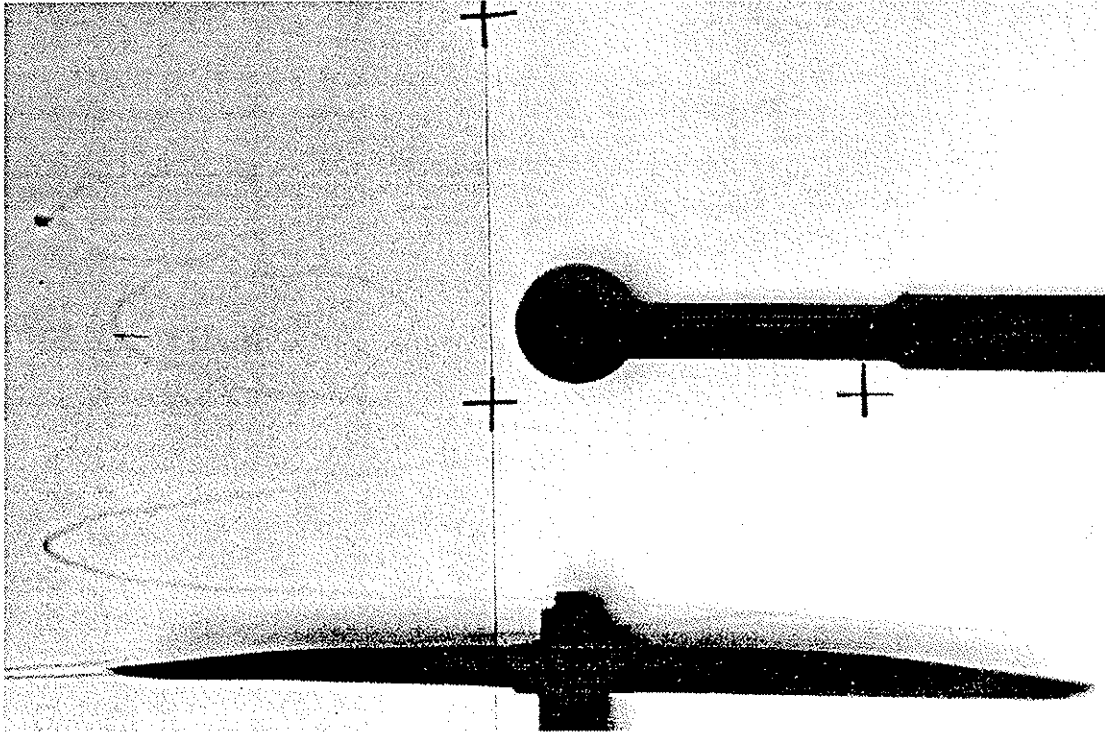


Figure 11: Shadowgraph of rotor tip vortex/body interaction (view along longitudinal axis of body). Later time: Note vortex bursting.

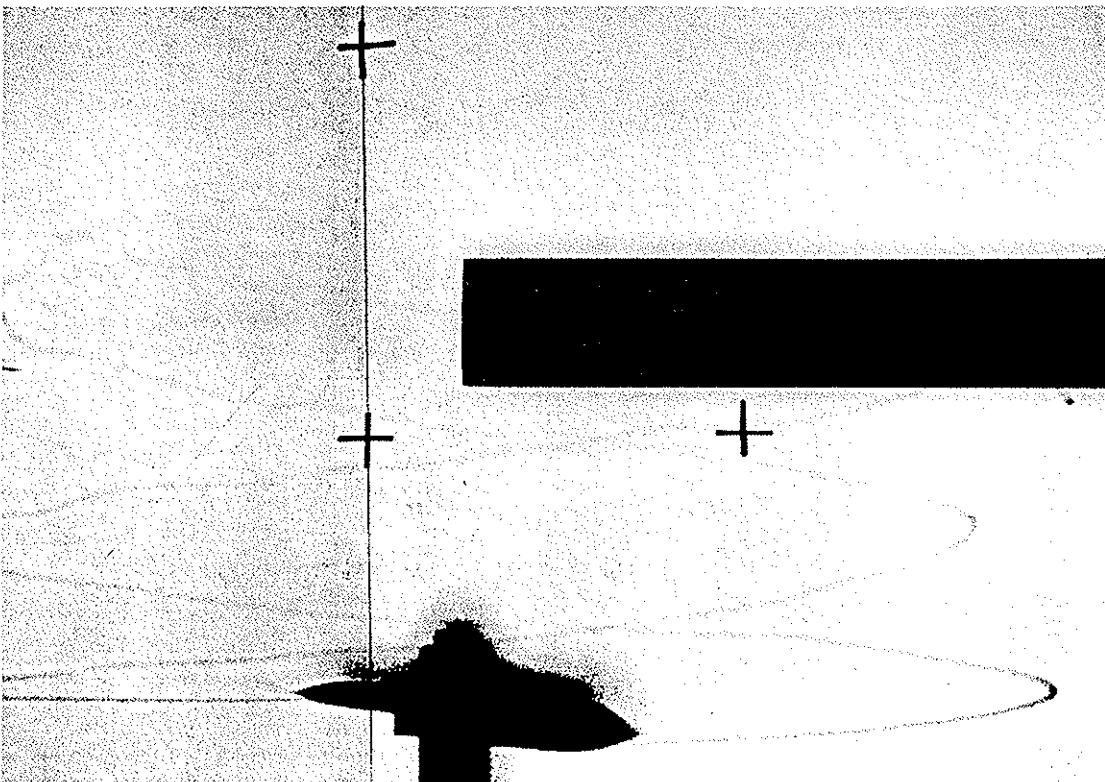


Figure 12: Shadowgraph of rotor tip vortex/body interaction (side view)

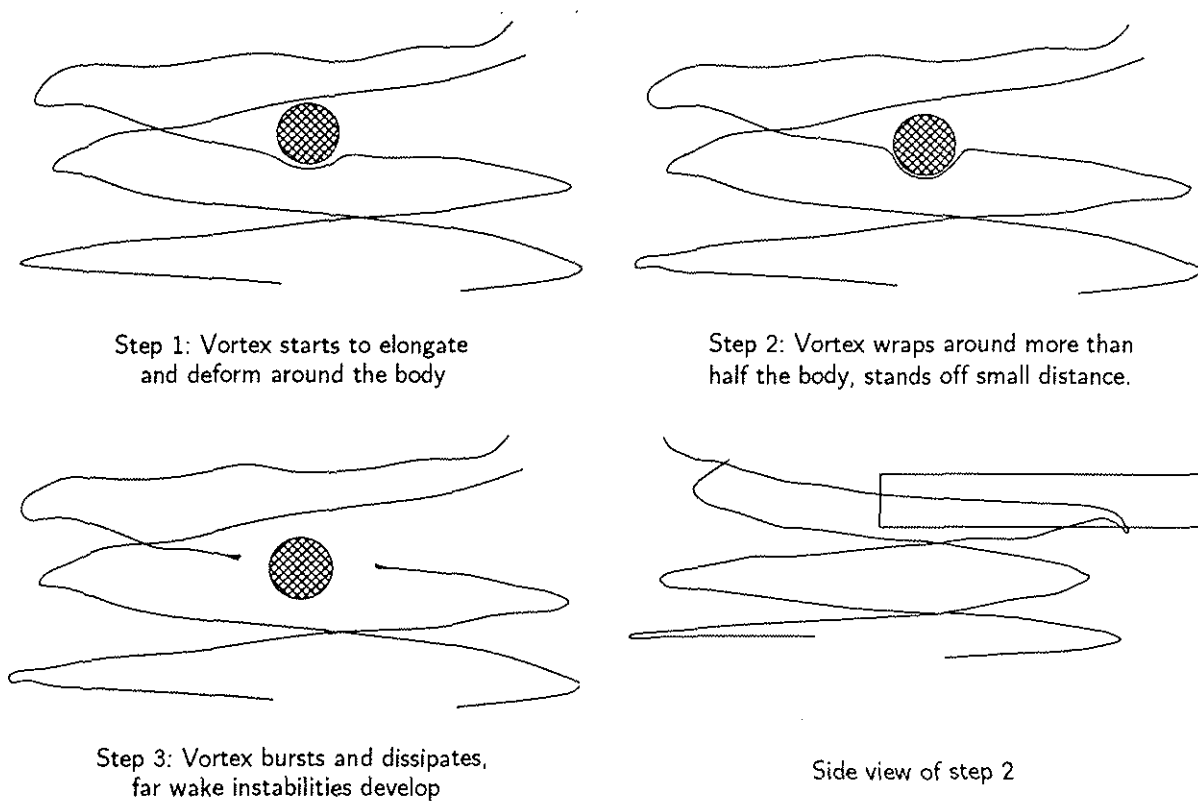


Figure 13: Schematic of rotor tip vortex/body interaction process

As the wake is convected further, the vortex filament becomes significantly strained and it could be seen to begin to diffuse. Two "ends" of the vortex filament, one on each side of the body, could be observed, and the diffusion gradually spread along the length of the filament for increasing time. This process was particularly vivid when recorded on video tape. This overall process resulted in the destruction of the discrete tip vortices, and no evidence could be seen of the filaments "reconnecting" below the level of the body. A schematic of the entire process is shown in Fig. 13.

Descent Conditions

Classically, the flow through a rotor is characterized by three states, as determined by the relationship of the average rotor induced velocity, v_i , to the axial velocity of the rotor, v_c . Hovering ($v_c = 0$) and climbing ($v_c > 0$) share the normal working state where the flow is everywhere downward through the rotor disk. For a rotor descending at a rate greater than $2v_i$, the flow is upward and the rotor operates in the windmill brake state. Both the normal working state and windmill brake states are smooth flows with a definite slipstream boundary. Between these states, the rotor is operating in the vortex ring state, and experiences highly unsteady flow with regions of concurrent upward and downward flows through the disk. The flow states appear to have been first described by Lock *et al.*,³² and were later confirmed by Drees and Hendal³³ using smoke flow visualization. However, there appears to have been no subsequent experiments that have documented the detailed locations of the tip vortices under these conditions.

To examine the flow state under simulated descent conditions, the small-scale rotor assembly was mounted horizontally and located in the working section of an open jet wind tunnel. The rotor axis was aligned with the centerline of the wind tunnel. By varying the speed of the flow from the wind tunnel, various descent conditions could be obtained. For these experiments, the rotor was maintained at a rotational speed of 240 Hz (14,400 RPM), which produced a tip Mach number of about 0.63.

Figs. 14, 15, and 16 show some typical shadowgraphs of the wake in different descent conditions. For low rates of descent, the tip vortex filaments remained closer to the plane of the rotor than for the hover case, but were convected radially outward. At slightly higher descent rates, the tip vortices remained even closer to the rotor plane, but considerable unsteadiness was also introduced. This is

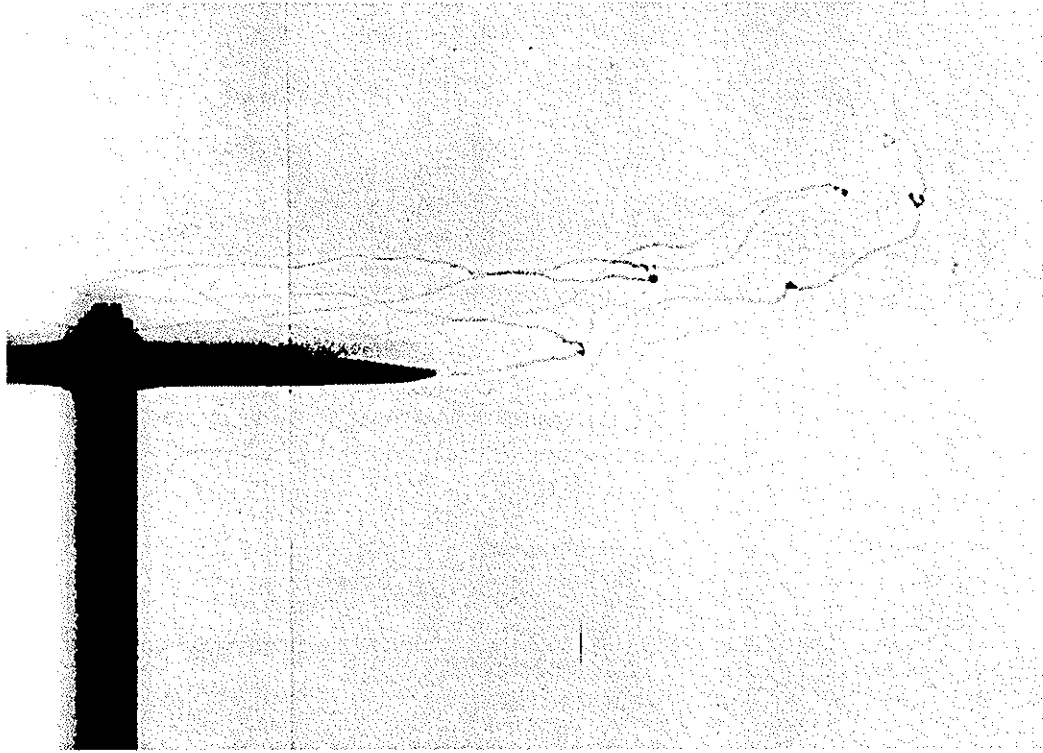


Figure 14: Sample shadowgraph of wake in descent condition, $M_{tip} = 0.63$, $v_c/v_h \approx -1.9$.

evidenced in the shadowgraphs by the considerable twisting and folding of the tip vortices, and the lack of any distinct slipstream boundary. Significant vortical wake geometry variations with azimuth indicated a high degree of unsteadiness.

If the descent velocity was increased further, the wake was seen to develop a definite slipstream boundary that expanded downstream of the rotor, as typical of the windmill brake state. Once transitioned to the windmill brake state – see Fig. 16 – the vortical chaos disappeared and the wake structure returned to a more helical structure. The overall transition from hover to the windmill brake state is illustrated in Fig. 17. This figure is a composite made from many shadowgraphs and schlierens which shows the averaged wake boundaries for different descent velocities. By convention, the descent velocity was non-dimensionalized with respect to the averaged rotor induced velocity in hover. Note that for v_c/v_h about -1.8, there is a pronounced recirculation in the flow, and this is essentially the vortex-ring state.

5. CONCLUDING REMARKS

A series of shadowgraph and schlieren studies have been performed to visualize the wakes of small scale rotors operated at full-scale tip Mach numbers. The study has given a better appreciation of the various flow problems that could be studied on propeller and rotors using these techniques. Various optical and photographic techniques were also explored, with a view to optimizing the techniques for rotor applications. Studies were conducted in hover and in axial descent, along with a study of rotor wake/body interactions.

The following conclusions have been drawn from this work:

1. While the schlieren technique appears more sensitive than the shadowgraph technique, the latter must be preferred for rotorcraft work. The additional effort and complications required to precisely align sensitive optics yields only marginally better results, and can be marred by problems such as astigmatism and coma. In addition, the larger field of view of the shadowgraph method caters more to the requirements of the rotorcraft researcher.
2. The best photographic results were obtained using the shadowgraph method with a beam splitter arrangement. However, every effort should be made to keep the light source as close to a point source as possible, and to keep incident viewing angles to less than 30 degrees.

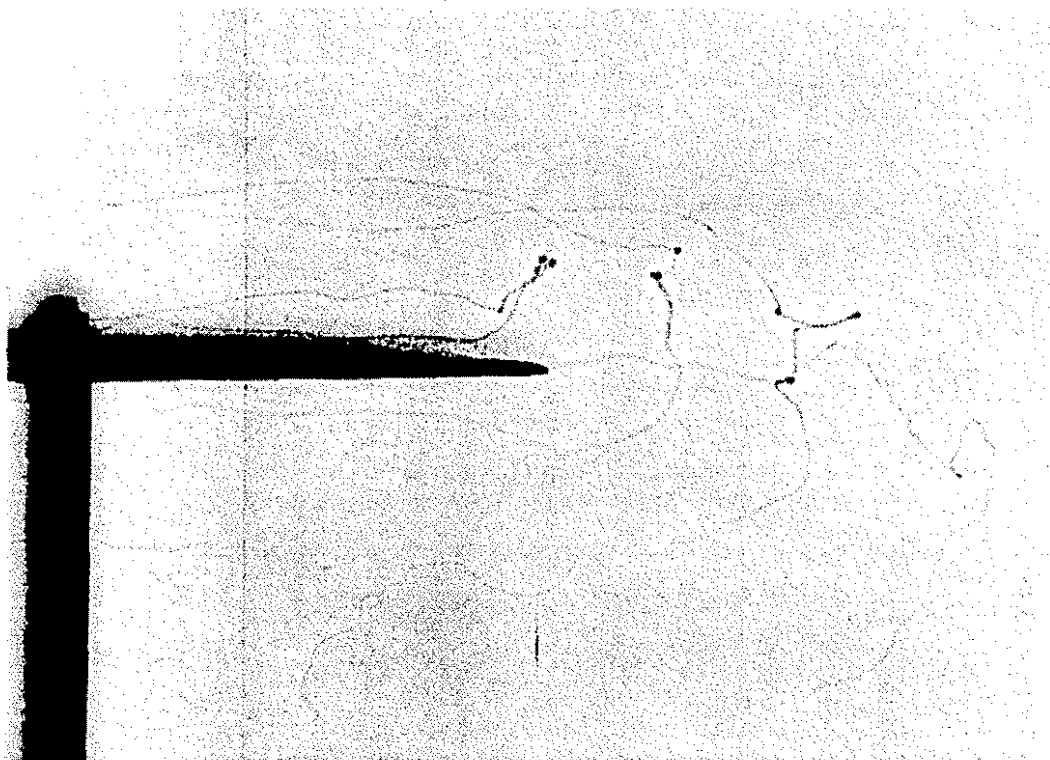


Figure 15: Sample shadowgraph of wake in descent condition, $M_{tip} = 0.63$, $v_c/v_h \approx -1.9$.

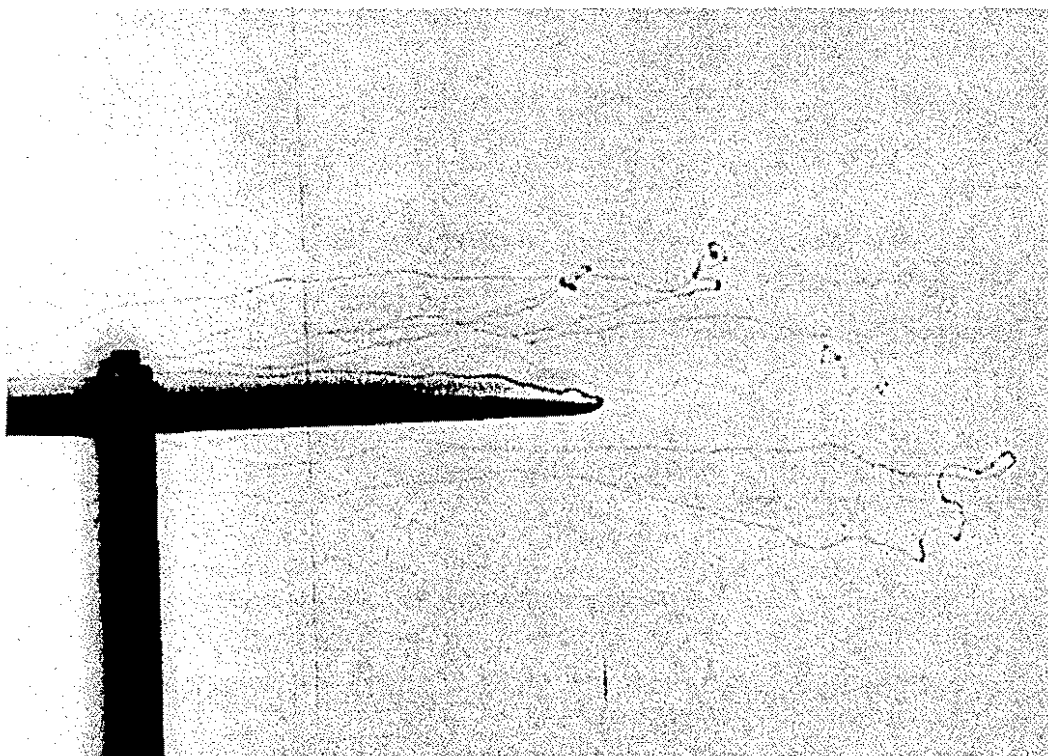


Figure 16: Sample shadowgraph of wake in descent condition, $M_{tip} = 0.63$, $v_c/v_h \approx -2.0$.

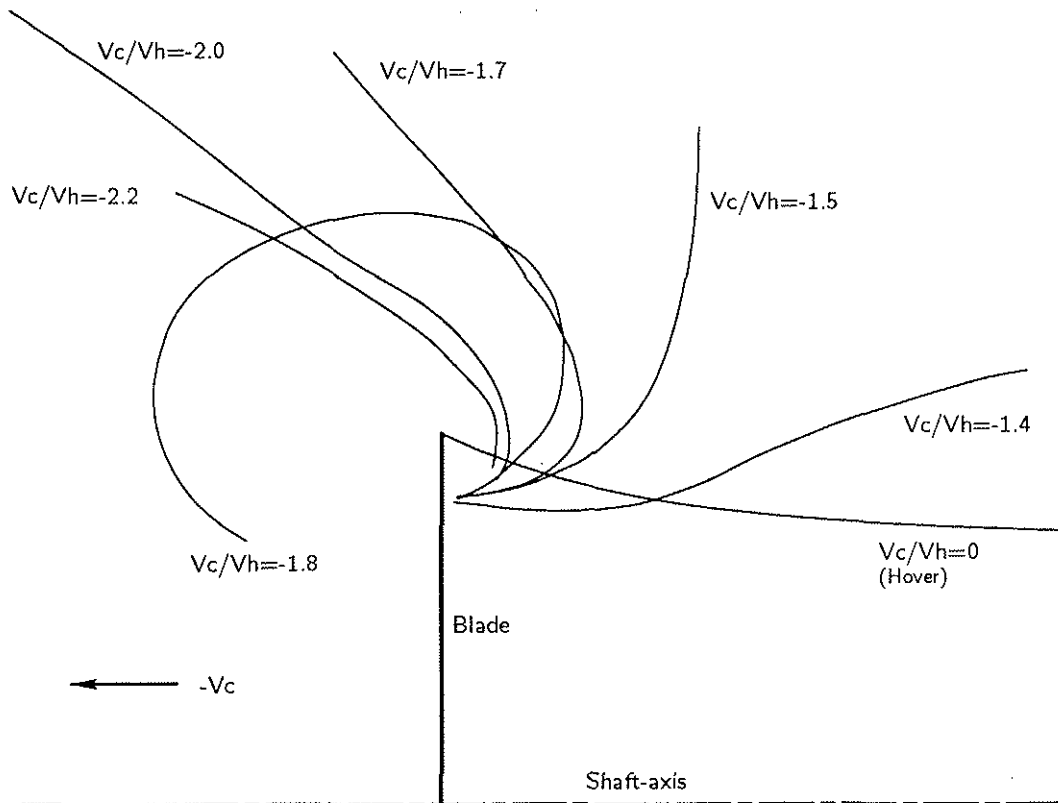


Figure 17: Rotor wake boundary at various rates of descent

3. As part of the studies, an interesting bi-stable flow state was discovered in the wake of a propeller. No solid explanation for the phenomenon has been found, and the matter should be the subject of future research.
4. Investigation of rotor/body interactions revealed that the vortices weaken somewhat in the presence of a body, yet remain visible. The tip vortices were found to stretch around the body, and eventually undergo breakdown. The concentrated vorticity in the tip vortices was then diffused into the wake.
5. Vertical descent conditions were simulated by placing the rotor assembly in a wind-tunnel. From the flow field images, the time-averaged locations of the wake boundaries could be obtained and plotted. The resulting information confirmed the existence of the so-called vortex-ring state, and the presence of flow recirculation near the rotor plane.

ACKNOWLEDGMENTS - This work was supported by the US. Army Research Office under contract DAAH-04-93-G-001. The authors appreciate the loan of the Task motor from the Glenn L. Martin wind-tunnel for use in these experiments. Particular thanks are due to Andrew Baker and Ashish Bagai who helped in the experiments.

REFERENCES

- [1] D.W. Boatwright, "Measurements of Velocity Components in the Wake of a Full-Scale Helicopter in Hover," USAAMRDL TR 72-33, 1972
- [2] F.X. Caradonna, C. Tung, "Experimental and Analytical Studies of a Model Helicopter Rotor in Hover," Paper No. 4, *7th European Rotorcraft Forum*, Garmisch-Partenkirchen, F.R.G., Sept. 1981.

- [3] J.C. Biggers, K.L. Orloff, "Laser Velocimeter measurements of the Helicopter Rotor Induced Flowfield," *Proceedings of the 30th Annual Forum of the American Helicopter Society*, Washington D.C., May 7-9, 1974.
- [4] H.H. Heyson, S. Katzoff "Induced Velocities Near a Lifting Rotor with Non-Uniform Disk Loading," NACA TR 1319, 1957.
- [5] I.C. Cheeseman, C. Haddow, "An Experimental Investigation of the Downwash Beneath a Lifting Rotor and Low Advance Ratios," *Vertica*, Vol. 13, No. 4, 1989, pp. 421-445.
- [6] Leishman, J.G., Bi, Nai-pei, "Measurements of a Rotor Flowfield and the Effects of a Fuselage in Forward Flight," *Vertica*, Vol.14, No. 3, 1990.
- [7] B. Junker, H.J. Langer, "Helicopter Rotor Downwash: Results of Experimental Research and Comparison with some Theoretical Results," *Vertica*, Vol. 7, No. 1, 1983, pp. 61-70.
- [8] S.L. Althoff, J.W. Elliott, R.H. Sailey, "Inflow Measurements made with a Laser Velocimeter on a Helicopter Model in Forward Flight," NASA Technical Memorandum 100544, April 1988.
- [9] C.V. Cook, "The Structure of the Rotor Blade Tip Vortex," AGARD CP-111, 1972.
- [10] C. Tung, S.L. Pucci, F.X. Caradonna, H.A. Morse, "The Structure of Trailing Vortices Generated by Model Helicopter Rotor Blades," *Vertica*, Vol. 7, No.1, pp. 33-43, 1983.
- [11] R. Piziali, A. Trenka, "An Experimental Study of Blade Tip Vortices," Report AC-2647-S-1, Cornell Aeronautical Laboratory, Buffalo, NY, 1970.
- [12] R.H. Spencer, "Application of Vortex Visualization Test Techniques to Rotor Noise Research," *Proceedings of the American Helicopter Society 26th Annual Forum*, Washington, DC, 1970.
- [13] B.D. Leighty, D.B. Rhodes, J.M. Franke, S.B. Jones, "A Synchronous Strobed Laser Light Sheet for Rotor Flow Visualizations," NASA TM-4266, 1991.
- [14] T.A. Ghee, J.W. Elliott, "A Study of the Rotor Wake of a Small-Scale Rotor Model in Forward Flight using Laser Light Sheet Flow Visualization with Comparisons to Analytical Models," *Proceedings of the American Helicopter Society 48th Annual Forum*, Washington, DC, 1992.
- [15] F.F. Felker, M.D. Maisel, M.D. Betzina, "Full-Scale Tilt-Rotor Hover Performance," *Journal of the American Helicopter Society*, Vol. 31, Vol. 2, pp. 10-18, 1986.
- [16] W.F. Hilton, "The Photography of Airscrew Sound Waves," *Royal Society of London*, Series A, Vol. CLXIX, 1939.
- [17] J.L. Tangler, "Schlieren and Noise Studies of Rotors in Forward Flight," *Proceedings of the American Helicopter Society 33rd Annual Forum*, Washington, DC, 1977.
- [18] T.R. Norman, J.S. Light, "Rotor Tip Vortex Geometry Measurements Using the Wide-Field Shadowgraph Technique," *Journal of the American Helicopter Society*, Vol. 32, No. 2, pp. 40-50, 1987.
- [19] A. Bagai, J.G. Leishman, "Improved Wide-Field Shadowgraph Set-up for Rotor Wake Visualization," *Journal of the American Helicopter Society*, Vol. 37, No. 3, pp. 86-92, 1992.
- [20] S.P. Parthasarthy, Y.I. Cho, L.H. Black, "Wide-Field Shadowgraph Flow Visualization of Tip Vortices Generated by a Helicopter Rotor," Paper 85-1557, *AIAA 18th Fluid Dynamics and Plasmadynamics and Lasers Conference*, Cincinnati, OH, 1985.
- [21] J.S. Light, "Tip Vortex Geometry of a Hovering Helicopter Rotor in Ground Effect," *Proceedings of the 45th American Helicopter Society*, Boston, MA, 1989.
- [22] J.G. Leishman, A. Bagai, "Rotor Wake Visualization in Low Speed Forward Flight," AIAA paper 91-3232, *AIAA 9th Applied Aerodynamics Conference*, Baltimore, MD, 1991.
- [23] D.W. Holder, R.J. North, "Schlieren Methods," Notes on Applied Science, No. 31, Dept. of Scientific and Industrial Research, National Physical Laboratory, HMSO, London, 1963.

- [24] J.H. Goncz, P.B. Newell, "Spectra of Pulsed and Continuous Xenon Discharges," *Journal of the Optical Society of America*, Vol. 56, No.1, pp. 87-92, 1966.
- [25] Ilford Photo Corporation, "Technical Information: 400 Delta," Catalog # 9446, Paramus, NJ, 1991.
- [26] Ilford Photo Corporation, "Technical Information: HP5 Plus," Catalog # 8701, Paramus, NJ, 1992.
- [27] Eastman Kodak Company, "Kodak TMAX Professional Films," Kodak Publication F-32, Rochester, NY, 1991.
- [28] Ilford Photo Corporation, "Technical Information: XP2," Catalog # 9444, Paramus, NJ, 1992.
- [29] Eastman Kodak Company, "Kodak Infrared Films," Kodak Publication N-17, Rochester, NY, 1981.
- [30] Bi, Nai-pei, Leishman, J. G., "Experimental Study of Aerodynamic Interactions between a Rotor and a Fuselage," *Journal of Aircraft*, Vol. 27, No. 9, Sept. 1990.
- [31] Bagai, A., Leishman, J.G., Samak, D.K., "A Study of Rotor Wake Development and Wake/Body Interactions in Hover," Vol. 37, No. 4, *Journal of the American Helicopter Society*, Oct. 1992.
- [32] C.N.H. Lock, H. Bateman, H. Townend, "An Extension of the Vortex Theory of Airscrews with Applications to Airscrews of Small Pitch and Including Experimental Results," Reports and Memoranda No. 1014, British Aeronautical Research Committee, 1925.
- [33] J.M. Drees, W.P. Hendaal, "The Field of Flow through a Helicopter Rotor Obtained from Wind Tunnel Smoke Tests," Report No. V-1205, Nationaal Lucht- en Luchtvaart Laboratorium, Amsterdam, 1950.